IEEE Access
Multidisciplinary ⋮ Rapid Review ⋮ Open Access Journal

Received 19 July 2023, accepted 7 August 2023, date of publication 14 August 2023, date of current version 17 August 2023.

Digital Object Identifier 10.1109/ACCESS.2023.3304697

RESEARCH ARTICLE

Model Predictive Control Method of Multi-Energy Flow System Considering Wind Power Consumption

QILONG ZHANG[1], XIANGPING CHEN[2], GUANGMING LI[1], JUNJIE FENG[1], AND ANQIAN YANG[3]

[1]School of Physics and Electrical Engineering, Liupanshui Normal University, Liupanshui 553004, China
[2]Guizhou University, Guiyang 550025, China
[3]Electric Power Research Institute, Guizhou Power Grid Company Ltd., Guiyang 550025, China

Corresponding author: Qilong Zhang (384198892@qq.com)

This work was supported in part by the Natural Science Research Project of Guizhou Provincial Education Office under Grant Qianjiaohe KY Zi [2022] 047, in part by the Natural Science Research Project of Scientific Research Project of Liupanshui Normal University under Grant LPSSYZK202013, in part by the Research Project of Liupanshui Normal University under Grant LPSSYYBZK202203, in part by the Construction Project of First-Class Discipline of Liupanshui Normal University under Grant LPSYylbkzy202007, and in part by the Guizhou Province First-Class Undergraduate Major Construction Project under Grant GZSylzy202101.

ABSTRACT In recent years, global energy shortages and environmental pollution have intensified. With the large-scale development of new energy wind energy, there is also a major problem-insufficient absorption capacity. In order to promote large-scale wind power consumption, a model predictive control method based on wind hydrogen coupled power generation system is proposed. Firstly, the mathematical models of equivalent state of charge in wind power, hydrogen energy storage systems (HESS), and gas storage tanks are analyzed. Secondly, the optimization objective function is to maximize the local wind energy consumption and minimize the energy interaction between the main grid. Establish an SSM prediction model based on the MPC strategy. Genetic optimization algorithm is used for rolling solution. Aiming at the interference and prediction error generated during the operation of the system, a feedback mechanism is introduced to embed it into the MPC framework. Then, the rolling time domain method is used to compensate for system interference. Finally, a case study was conducted based on actual measurement data from a certain area in the Netherlands. By comparing the wind power dissipation effects of the system during operation, it is verified that the proposed method can effectively reduce interactive power consumption. Maximize the local consumption of wind power.

INDEX TERMS Wind power consumption, multi-energy flow system, HESS, MPC optimization method.

I. INTRODUCTION

Energy is the foundation of human existence and national economy. At the same time of economic development, with the increasing demand for electric energy in the world, the conventional power generation mode with high consumption and high pollution is no longer suitable for the social development concept [1]. Under the dual pressure of energy demand and climate environment, it is urgent to improve the penetration rate of renewable energy distributed power [2].

The associate editor coordinating the review of this manuscript and approving it for publication was Yonghao Gui.

According to statistics, the use of the three non-renewable resources (crude oil, natural gas and coal) currently used on the earth is about to be exhausted, and the mining life is gradually increasing, which is 39 years, 50 years and 239 years respectively [3]. The amount of harmful gases emitted by the combustion of these three types of non-renewable energy is staggering, with 32 billion tons of carbon dioxide, 120 million tons of sulfur dioxide and 110 million tons of nitrogen oxide. Such a large amount of harmful gases have brought serious harm to the ecosystem [4], [5], [6], [7], [8]. The renewable energy reserves to be mining output are abundant. At present, the wind, water and solar energy reserves to be mining

output account for 99.95% of the reserves, and the clean resource reserves are even more abundant. The world's wind, water and solar energy reserves are respectively 1, 100 and 100 trillion kilowatts [9]. It can be seen that the large-scale development and utilization of renewable energy can solve human energy needs.

Wind energy is an inexhaustible renewable energy, but wind energy is dynamic, so large-scale grid connection is limited, resulting in many abandoned wind. The combination of wind energy and hydrogen energy storage is a way to increase wind power consumption, because the electrolytic water device can adapt to the unstable output of wind power [10]. The wind power that cannot be used in the grid can be converted into hydrogen through the electrolytic water device for storage (which can be stored for a long time). The hydrogen can also be used for fuel cells to generate electricity to return to the grid and suppress the fluctuation of the grid. There are many studies on wind power combined with hydrogen storage and consumption of wind power. In order to achieve the goal of maximizing the local consumption of wind power, the literature [11] has established a multi-functional coupling system of three kinds of energy, based on the efficient use of energy and the goal of low carbon content, combined wind power and coal chemical industry, and established a functional mathematical model through the connection of hydrogen energy system. The constraint conditions used in this mathematical model are the maximum utilization rate of wind power and stable operation. According to the genetic optimization algorithm, the feasible operation scheme of the system is obtained. Literature [12] designs a hybrid system that operates automatically in off-grid state. From the test results of real-time operation, the hybrid solar/battery system with standby syngas generator unit is more reliable and can meet the changing power demand. The operation strategy of this generator unit is based on the state of charge (SOC) of the battery, and the generator unit is in the self-starting state, to power the load by generating electricity. When the SOC drops to 40%, charge it until the SOC recovers to 80%. For the energy problem in remote Xinjiang, the document [13] proposes a set of hybrid energy systems including wind power generation, hydrogen energy storage, utilization of coal, and rational use of solar energy. According to the geographical location of Hami, Xinjiang, it proposes to use wind and solar energy, and establish its optimization model to maximize the local consumption of wind and solar energy.

Model predictive control (MPC) is widely considered as a very effective method for systems with high uncertainty, multi disturbance and multi unknown parameters. It has a wide range of applications, such as food processing, irrigation systems, robots, building ventilation, unmanned vehicles, etc. MPC corrects the error by continuously detecting the error between the predicted value and the real value online in the closed-loop control system, to ensure the stability of the control system.

In addition, MPC energy management method is an advanced energy management technology, which can help enterprises and individuals manage energy consumption more effectively, thereby reducing energy costs and environmental impact. MPC can realize the optimal control of energy consumption through the modeling and prediction of energy system, to realize the efficient utilization of energy. In recent years, the combination of MPC and GA can realize the optimization of different energy forms [14], [15], and as a research method to study the optimal control of power system, it has received extensive attention [16], [17], [18], [19].

With regard to the research of model predictive control (MPC) method, literature [20] proposed a model predictive control method based on home energy LAN in its article. This method can reduce the cost of household consumption by optimizing the allocation of effective combination of micro-sources in the home LAN to improve the utilization rate of renewable energy. Literature [21] studies and analyzes the optimal scheduling scheme of microgrid energy based on conventional economic optimal scheduling, and proposes a new scheduling scheme with multiple time scales. During the period of power grid operation every day, the distribution and adjustment of different electricity usage and the amount of electricity price in different time periods are carried out. However, this multi-time scheduling method also lacks the feedback part and the rolling optimization of MPC, and the whole scheduling process is relatively rigid. Literature [22] takes the minimum operation cost of the microgrid as the objective function for optimization. For the microgrid of the energy storage system composed of sodium sulfur batteries, an energy management strategy with multiple operation optimization time scales is proposed, and particle swarm optimization is used to solve the timescale models. The literature [23] uses multi-time scale predictive control for the optimal scheduling of microgrid energy. The optimal cost control is used when the timescale is the upper and lower slow scale, and the overall electricity demand is mainly satisfied when the timescale is the lower fast scale. Document [24] uses the control method of distributed predictive control to put forward the strategy and method of dispatching according to the electricity price parameters of each period. In the microgrid control management, the dual analysis is used to plan the whole structure into a two-level dispatching structure, and the Lagrange coordination factor is used for the purpose of optimal solution. Literature [25] adopts the model predictive control method to coordinate and optimize the microgrid energy storage device and diesel generator, improve the maximum wind energy consumption of the microgrid system, and minimize the abandoned air volume of the microgrid system.

In addition, in order to improve the utilization rate of energy, document [26] proposed an indirect multi energy trading method based on deep learning, which is realized through the personalized response of self energy on the basis of promoting the multi energy collaborative optimization

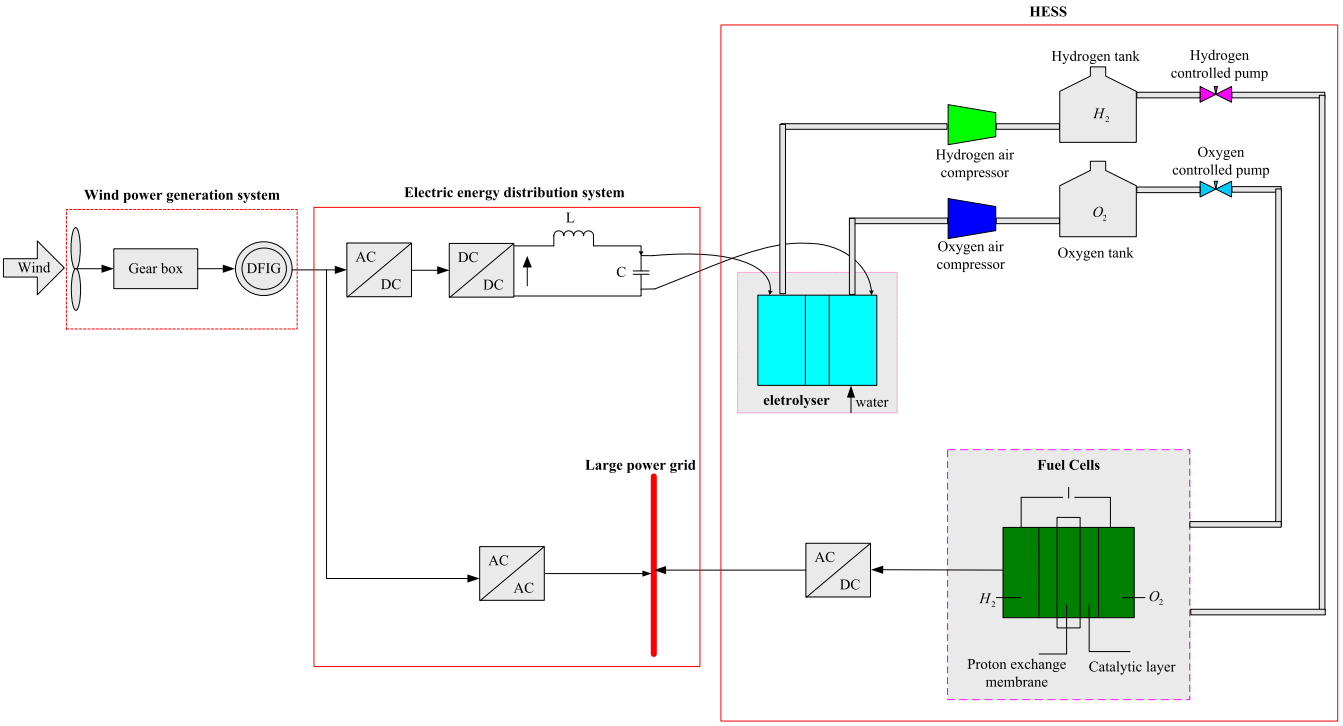

FIGURE 1. Systematical diagram of a multi-energy system.

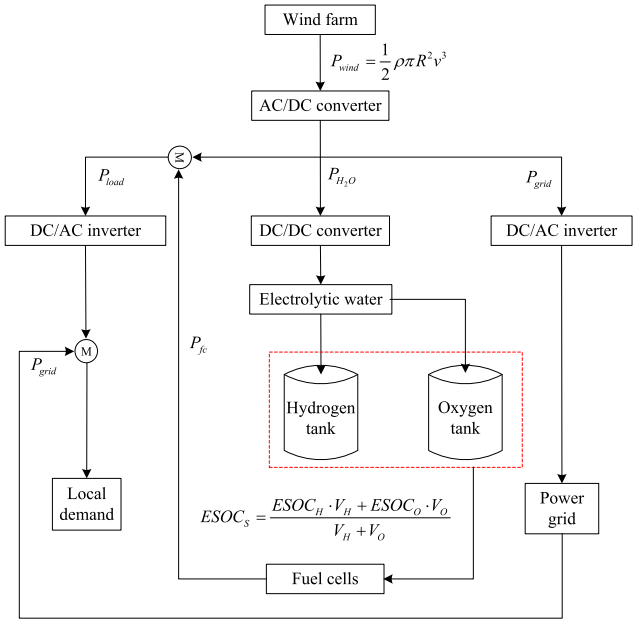

FIGURE 2. A flow chart of the multi-energy system.

in the local energy market. Reference [27] proposed a distributed multi energy flow calculation method based on fixed points for the multi energy flow calculation problem. The method has good effect in calculation time, accuracy and robustness against data loss. In order to further enhance the adaptability and flexibility of multi energy flow system, [28] proposed an energy management method for multi energy system based on distributed dynamic trigger Newton Rawson algorithm. In order to alleviate the shortage of natural gas supply in winter, [29] proposed a medium and long-term energy optimization method for urban multi energy flow system considering seasonal peak shaving of natural gas.

The above literature has carried out various research work on multi energy flow system and its energy management. Although multi-level coordination and gradual refinement of scheduling strategy can largely absorb the fluctuation of intermittent energy and load, this open-loop optimal scheduling process does not consider the feedback correction of the actual system to the optimal control process. Therefore, based on the mathematical model of equivalent state of charge in wind power generation, hydrogen energy storage system and gas storage tank, the energy optimization of the system is studied and analyzed based on the model predictive control method. That is to build a state-space prediction model (SSM prediction model), establish a multi-energy flow system optimization model with the goal of minimum interaction between the system and the large grid (maximum absorption of local wind power), and use genetic algorithm for rolling solution, aiming at the interference and prediction error generated during the operation of the system, correct the control accuracy of the system by embedding feedback correction. Finally, an example shows that this method can effectively improve the level of wind power consumption, reduce wind abandonment, and realize the optimal energy flow control of the maximum consumption of local wind power.

II. DESCRIPTION OF MULTI-ENERGY FLOW SYSTEM

In order to absorb more wind power, the multi-energy flow system built in this paper is shown in Fig. 1. The system is composed of three subsystems, namely, wind power generation system, electric energy distribution system and hydrogen energy storage system. The electric energy distribution system controls the flow direction of wind power, including three paths, namely, local load consumption, water consumption and grid connection. The hydrogen energy storage system is composed of an electrolytic water device and a fuel cell, which mainly simulates the charging and discharging principle of the battery. The charging is equivalent to the hydrogen production from electrolytic water to absorb wind power, and the discharging is equivalent to the hydrogen generation from the fuel cell. Electricity and gas coupling among the three subsystems, wind power generation system, power distribution system, and hydrogen energy storage system ''cache'' wind power. First, wind power can be supplied to the local load for consumption, and the surplus wind power can be supplied to the electrolytic water for hydrogen production and storage, and then the remaining wind power can be connected to the grid for consumption. If the wind power is too small and the wind power cannot meet the load, then the fuel cell will consume the hydrogen stored temporarily during the high wind to supply the local load for consumption. If the load is still not met, the grid will supply again. The specific energy flow in the system is shown in Fig. 2.

III. MULTI-ENERGY FLOW SYSTEM MODEL

The purpose of establishing a system model is to quantitatively analyze the flow direction of system energy to determine the output of the system, specifically including the mathematical model of wind power output, the mathematical model of hydrogen energy storage system (electrolytic water hydrogen production model, the equivalent state of charge model in the gas storage tank, and the mathematical model of fuel cell output).

A. MATHEMATICAL MODEL OF WIND POWER OUTPUT

According to the relevant knowledge of air hydrodynamics, when the airflow passes through the wind turbine, assuming that the wind energy can be fully converted into mechanical energy, the mathematical model of wind power output can be presented in the form of formula (1):

$$P_m = \omega T_m = \frac{1}{2}\rho\pi R^2 \cdot v^3 \cdot C_f \tag{1}$$

where, P_m is the actual wind power (W).ρ is the air density ($kg \cdot m^3$). ω is the fan speed (rpm).v is the wind speed at the high position of the fan hub (m/s). T_m is the mechanical torque of the fan ($kg{\cdot}m$). R is the radius of the wind wheel (m). C_f is the wind energy utilization coefficient (dimensionless), the maximum value is 0.593.

The specific value of C_f can be calculated by the following formula (2):

$$\begin{cases} C_f(\gamma,\beta) = C_1\left(\dfrac{C_2}{\gamma_1} - C_2\beta - C_4\right)e^{-\frac{C_5}{\gamma_i}} + C_6\gamma \\ \dfrac{1}{\gamma_i} = \dfrac{1}{\gamma + 0.008\beta} - \dfrac{0.035}{\beta^3 + 1} \end{cases} \tag{2}$$

where, $C_1 \sim C_6$ is constant. γ is the tip speed ratio of the fan, $\gamma = \omega R/v$; β is the pitch angle.

B. MATHEMATICAL MODEL OF HYDROGEN ENERGY STORAGE SYSTEM

1) HYDROGEN PRODUCTION MODEL OF ELECTROLYTIC WATER

When electrolyzing water to produce hydrogen, under the standard state, according to the law of conservation of materials, the amount of hydrogen and oxygen produced in the process of electrolyzing water can be expressed by formula (3). The flow of hydrogen and oxygen produced is shown in formula (4).

$$\begin{cases} n_{H_2} = \dfrac{\eta_f \cdot n_{el} \cdot I_{el}}{2F} \\ \eta_f = 96.5 \cdot e^{\left(\frac{0.09}{I_{el}} - \frac{75.5}{I_{el}^2}\right)} \end{cases} \Rightarrow n_{O_2} = \frac{1}{2}n_{H_2} \tag{3}$$

$$\begin{cases} V_{H_2} = 2V_{O_2} = 418 \cdot P_s \cdot \dfrac{\eta_f}{U_s} \\ U_s = U_q + \dfrac{r_1 + r_2 \cdot T_{el}}{A_{el}} \cdot I_{el} + \left(s_1 + s_2 \cdot T_{el}^2\right) \cdot \\ \qquad \log\left(\dfrac{t_1 + \frac{t_2}{T_{el}} + \frac{t_3}{T_{el}^2}}{A_{el}} \cdot I_{el} + 1\right) \end{cases} \tag{4}$$

where, n_{H_2} and n_{O_2} is the amount of hydrogen and oxygen produced by electrolysis of water. n_{el} is the amount of electrolyte substance. U_s is the voltage at both ends of the electrolytic cell. P_s is the power flowing into the electrolytic cell. A_{el} is the electrode area, T_{el} indicates the electrolyte temperature. η_f is the electrolytic efficiency of the electrolytic cell. I_{el} is the equivalent current of the electrolytic cell. F is Faraday constant, just $F = 96485C/mol$. U_q indicates the reversible voltage of the electrolytic cell. V_{H_2} and V_{O_2} represent hydrogen flow (L/h) and oxygen flow (L/h) respectively. s_1, s_2, s_3, t_1, t_2, t_3 both represent electrode overvoltage parameters.

2) EQUIVALENT STATE OF CHARGE MODEL IN GAS STORAGE TANK

In this paper, the electrolytic water device, hydrogen and oxygen tank and fuel cell are combined to form an energy storage system. Hydrogen/oxygen consumption is similar to charging the battery. During the discharge process, fuel cells generate electricity by consuming hydrogen/oxygen, while hydrogen/oxygen gradually decreases. In order to evaluate the residual quantity in storage, the concept of equivalent state of charge [30], [31] (ESOC) is introduced, as shown in formulas (5), (6) and (7). In addition, for the safety of the gas

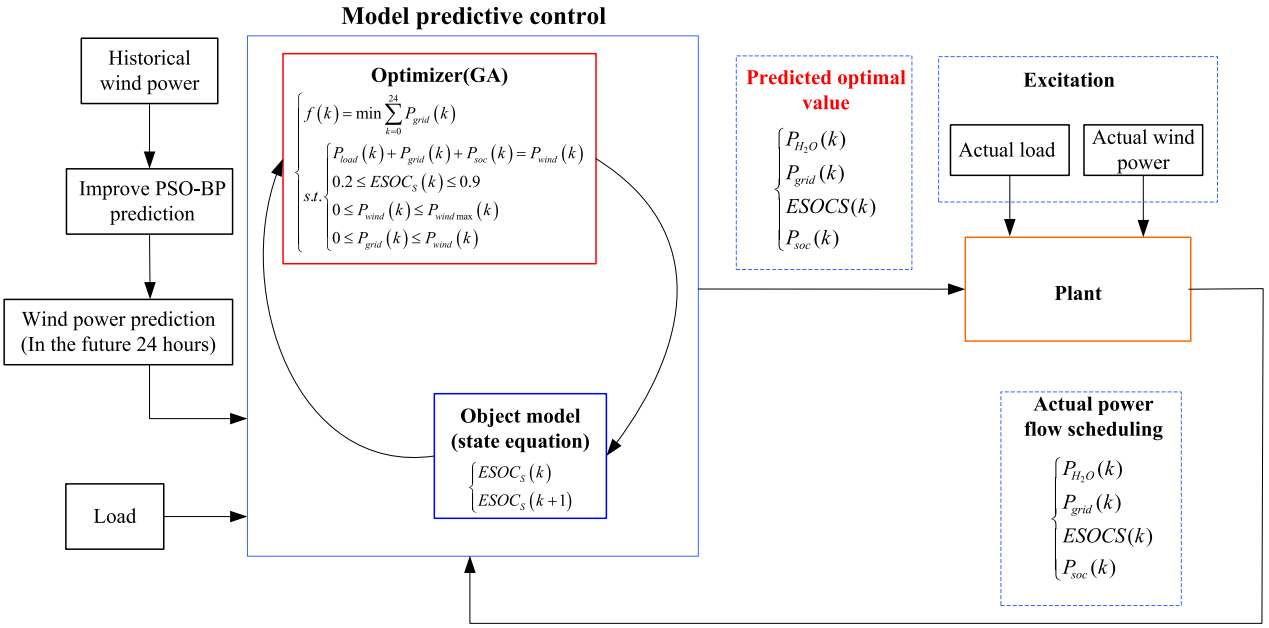

FIGURE 3. MPC strategy implementation process.

storage tank, the equivalent state of charge of the gas storage tank has a safe range (0.2 ∼ 0.9).

$$ESOC_H = \frac{P_{H_S}}{P_H^M} \tag{5}$$

$$ESOC_O = \frac{P_{O_S}}{P_O^M} \tag{6}$$

$$ESOC_S = \frac{ESOC_H \cdot V_H + ESOC_O \cdot V_O}{V_H + V_O} \tag{7}$$

where, $ESOC_H$, $ESOC_O$, $ESOC_S$ represent the equivalent state of charge of hydrogen tank, oxygen tank and hydrogen energy storage system respectively. P_{H_S}, P_{O_S} respectively represents the current residual pressure of hydrogen and oxygen storage tanks. P_H^M, P_O^M respectively represents the full pressure value of hydrogen and oxygen storage tank. V_H, V_O respectively represents the volume of hydrogen and oxygen storage tanks.

3) FUEL CELL OUTPUT MATHEMATICAL MODEL

The proton exchange membrane based fuel cell [32], [33], [34], [35], [36] (PEMFC) has a broad application prospect with high conversion efficiency, environmental protection and other characteristics. It can rapidly convert hydrogen and oxygen chemical energy into electrical energy, and can be connected with electronic converters of different power, and then connected to the large power grid. Due to irreversible loss, the actual output voltage E^{cell} of PEMFC is lower than its balance potential, which is caused by irreversible loss for many reasons. This kind of loss is usually called polarization or overvoltage, and mainly comes from the open circuit potential E^o, activation loss potential η^{act}, oh mic loss potential η^{ohmic} and concentration loss potential η^{con}. E^{cell} is a function of output current, temperature and reactant partial pressure, which can be expressed by formula (8):

$$\begin{cases} E^{cell} = E^o - \eta^{act} - \eta^{ohmic} - \eta^{con} \\ E^o = -\dfrac{(\Delta H - T\cdot\Delta S)}{n\cdot F} + R\cdot T\cdot\ln\left(\dfrac{P_{H_2}\cdot P_{O_2}^{0.5}}{P_{H_2O}}\right) \\ \eta^{act} = \dfrac{R\cdot T}{\alpha\cdot n\cdot F}\cdot\ln\left(\dfrac{i}{i^o}\right) \\ \eta^{ohmic} = i\cdot\dfrac{I_M\cdot\lambda_M}{A} \\ \lambda_M = \dfrac{181.6\cdot\left[1+0.03\cdot\left(\frac{i}{A}\right)+0.062\cdot\left(\frac{T}{303}\right)^2\cdot\left(\frac{i}{A}\right)^{2.5}\right]}{\left[\lambda-0.634-3\cdot\left(\frac{i}{A}\right)\cdot\exp\left(4.18\cdot\frac{T-303}{T}\right)\right]} \\ \eta^{con} = \dfrac{R\cdot T}{n\cdot F}\cdot\ln\left(1-\dfrac{i}{i^L}\right) \end{cases} \tag{8}$$

where, T is the battery operating temperature (K). ΔS is the total reaction entropy, and $\Delta S = 163.15\text{mol}\cdot\text{K}$. ΔH is the total reaction enthalpy, $\Delta H = \Delta G + T\cdot\Delta S$, ΔG is Gibbs free energy, and $\Delta G = 237.18\text{KJ/mol}$. n is the number of electrons per hydrogen molecule, $n = 2.\alpha$ is the charge transfer coefficient.R is Avogadro constant, $R = 8.134J/(\text{mol/K})$. F is Faraday constant, $F = 96485\text{C/mol}$.R_{ele} it is the electronic resistance (negligible) that causes obstruction in the battery. i^o is the exchange current density, i^L is the limiting current density, i is the current flowing through the battery, in A. A is the activated cell area of proton exchange membrane (m^2). I_M is the thickness of proton exchange membrane (m). λ_M is the film resistivity. λ Is membrane water content, constant. P_{H_2}, P_{O_2}, P_{H_2O} partial pressure of hydrogen, oxygen and water (Pa).

Then the output power of section N PEMFC P_{Nemst} is shown in formula (9):

$$P_{Nemst} = N \cdot i \cdot E^{cell} \tag{9}$$

IV. IMPLEMENTATION OF MPC STRATEGY IN MULTI ENERGY FLOW SYSTEM

MPC is a model-based closed-loop optimization control strategy. Its core links are internal model, control algorithm and reference trajectory, or predictive model, rolling optimization and feedback correction. Its principle is to predict the output of the system in a period of time according to the system model, and feedback the actual output to timely correct the control quantity, and repeat the above process to achieve rolling optimization [37], [38]. The advantage of MPC is that it does not require high accuracy of the system model, can consider various constraints, can deal with multi-objective optimization problems, and has good dynamic control performance [39].

Based on the above analysis of MPC strategies and ideas, for the multi-energy flow system built by the system, the MPC strategies of each information flow in the system are shown in Fig. 3 below [40]. It mainly consists of two parts: MPC controller (including optimization algorithm and prediction model) and controlled object. GA optimization algorithm is adopted for optimization algorithm, and state Space model is adopted for prediction model. Specific idea: according to the predicted wind power and real load (reference value) of the improved PSO-BP in the early stage, the prediction time domain is set to 24 hours, and only the value at the first moment of the optimal control scheme (predicted wind power, energy storage system power, energy storage system status and power grid power) of each sampling period (24 hours) is selected through the rolling solution (GA) to act on the actual system, combining with the actual measured value, there is a real feedback from the actual system (the actual load, the actual power of the energy storage system, the actual state of the energy storage system and the actual grid power), and the next state of the system calculated according to the system state space model (SSM) is taken as the initial state of the system at the next time, and so on. Based on the above, this method involves multiple time scales because it uses historical data to make predictions, and uses prediction data to solve and make decisions to act on the present.

A. IMPROVED PSO-BP PREDICTION ALGORITHM

Particle Swarm Optimization (PSO) is an intelligent algorithm based on population. In 1995, two American psychologists Eberhard and Kennedy proposed it based on the behavior of bird groups [41]. The basic idea of PSO algorithm is to simulate society. That is, consider a random solution as a member of the group (particle). This particle has its own position and running speed in the solution space. According to the actual problem, determine a constraint condition (fitness function). All particles fly at a certain speed in the solution space, and find the global optimal solution by following the current optimal solution.

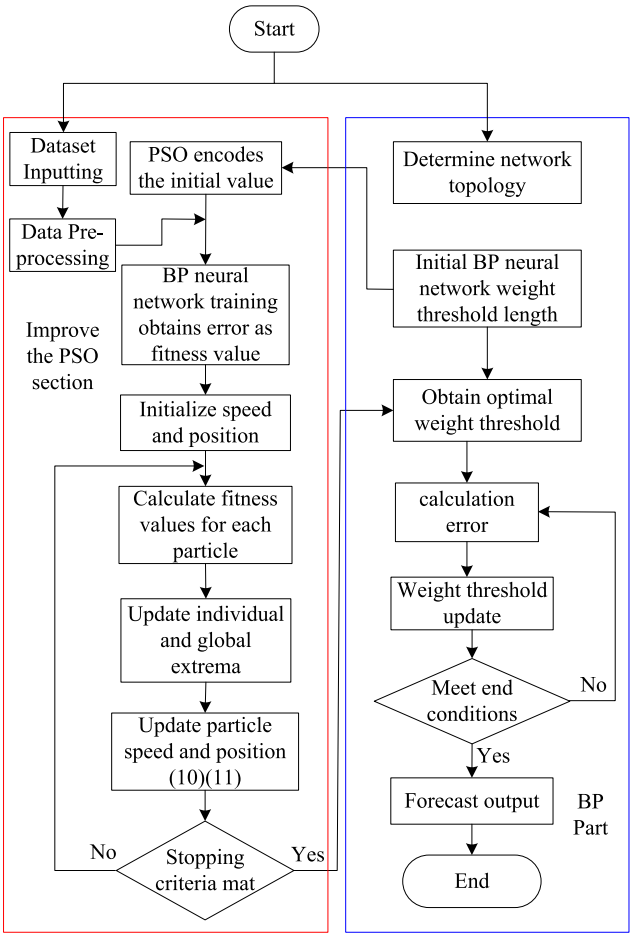

FIGURE 4. Flow chart of an improved PSO-BP algorithm.

Because of the specific super "inertia memory" ability of particles in conventional PSO (clustering to the spontaneous historical best, neighborhood, group historical best and other positions), the continuous aggregation leads to the phenomenon of rapid convergence effect of particle population, and finally is more likely to lead to the emergence of local extreme, premature convergence or stagnation and other defects, so in order to solve the above problems, the PSO is improved, That is, the adaptive inertia weight factor ω is introduced into the velocity update formula, and the gas is corrected to get the following formula (10), and the position update is as shown in (11):

$$v_{is}(t+1) = \omega \cdot v_{is}(t) + c_1 r_{1s}(t)\left[p_{is}(t) - x_{is}(t)\right] + c_2 r_{2s}(t)\left[p_{gs}(t) - x_{is}(t)\right] \tag{10}$$

$$x_{is}(t+1) = x_{is}(t) + v_{is}(t+1) \tag{11}$$

where,v_{is} is the flight speed of the ith particle in the s-dimensional target search space, $i = [1, m]$, $s = [1, S]$. c_1 and c_2 are learning factors and non negative constants. r_1 and r_2 are uniform random numbers in the range of [0,1].

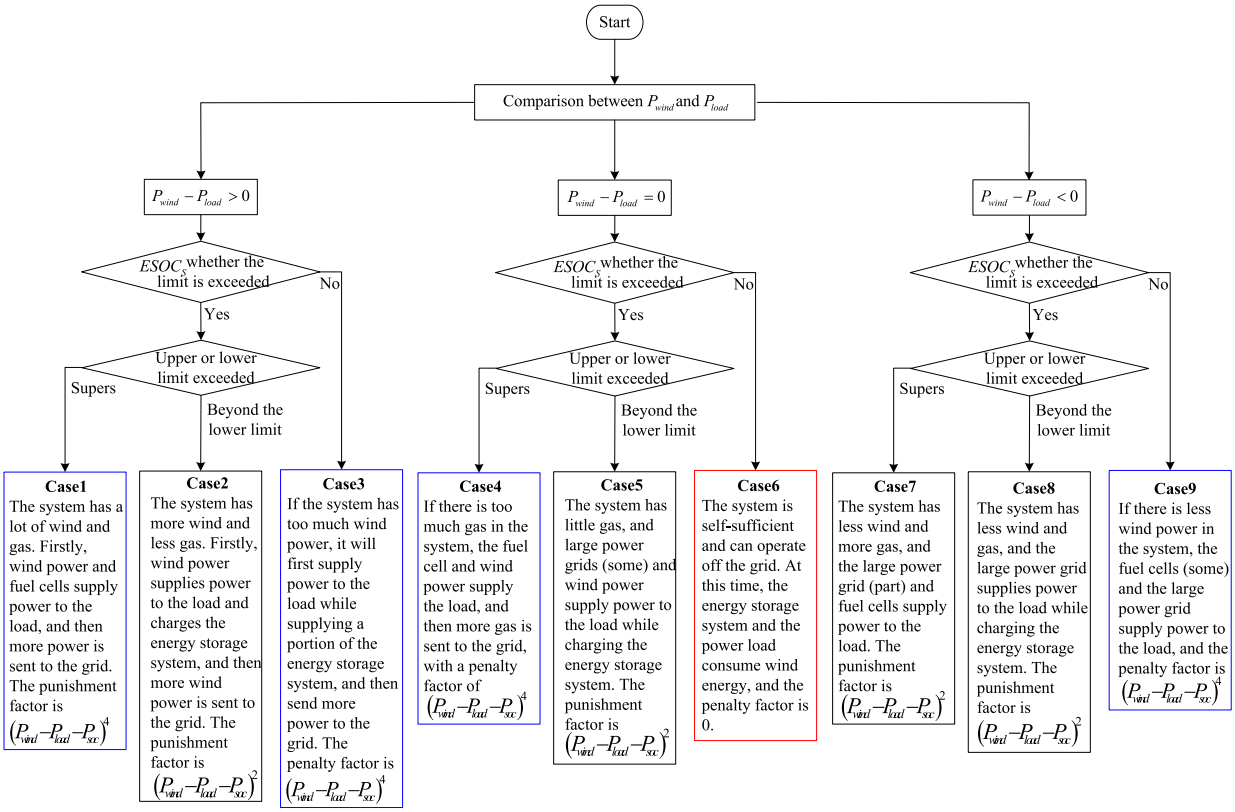

FIGURE 5. Nine cases of penalty definition.

x_{is} search the position of the ith particle in the space for the s-dimensional target. p_{is} is the optimal position searched by the ith particle. p_{gs} the optimal position for the whole particle swarm.

The value taking rule for ω is shown in formula (12):

$$\omega = \begin{cases} \omega_{\min} - \frac{(\omega_{\max}-\omega_{\min})*(f-f_{\min})}{f_{avg}-f_{\min}}, f \le f_{avg} \\ \omega_{\max}, f > f_{avg} \end{cases} \tag{12}$$

In the above formula, $\omega_{\max}$, $\omega_{\min}$ represents the maximum and minimum values of ω, f is the target value of particles at this time, and $f_{avg}, f_{\min}$ represents the average target value and the minimum target value of all particles in the whole process of motion (optimization).

The specific algorithm flow is shown in Fig. 4, and the specific algorithm description is as follows:

Step 1: According to the input and output sample sets and experience of the neural network, the topological structure of the network is 29-6-23-1.

Step 2: Random generation of initial weights and thresholds.

Step 3: The weights and thresholds of the neural network are coded. Mark individual particles in the form of real number vector.

Step 4: Initialization parameters.

The number of particles in the population $N = 100$, the maximum number of iterations $K_{\max} = 100000$, the acceleration factor $c_1 = c_2 = 1.49445$, the individual position $x_{\min}$, $x_{\max} \in [-5 \quad 5]$, and the flight speed $v_{\min}$, $v_{\max} \in [-1 \quad 1]$.

Step 5: Calculate the fitness value of each particle $Fit\,[t]$.

Step 6: Compare the optimal position $\overrightarrow{P_{iS}}$ searched so far by the ith particle with the optimal position $\overrightarrow{P_{gS}}$ searched so far by the whole particle swarm. If $Fit\,[t]$ is better than $\overrightarrow{P_{iS}}$, assign the value to $\overrightarrow{P_{iS}}$. Similarly, if $Fit\,[t] > \overrightarrow{P}_{gS}$, replace $Fit\,[t]$ with $\overrightarrow{P_{gS}}$.

Step 7: Update particle velocity v_i and position x_i according to formulas (10) and (11).

Step 8: Determination of termination conditions. If it is determined that it is satisfied, exit, and output the optimal weight and threshold, otherwise return to Step5.

B. SYSTEM MODEL CONSTRUCTION USING

In order to derive the relationship between the energy components of SSM in the system, the traditional state space model (SSM) expression describing the complex multi-vector energy system is used. In the system, the energy balance equation of the system can be expressed as:

$$P_{load}(k) + P_{H_2O}(k) = P_{fc}(k) + P_{grid}(k) + P_{wind}(k) \tag{13}$$

Assuming that the electrolytic water device and hydrogen and oxygen fuel are regarded as a whole - hydrogen

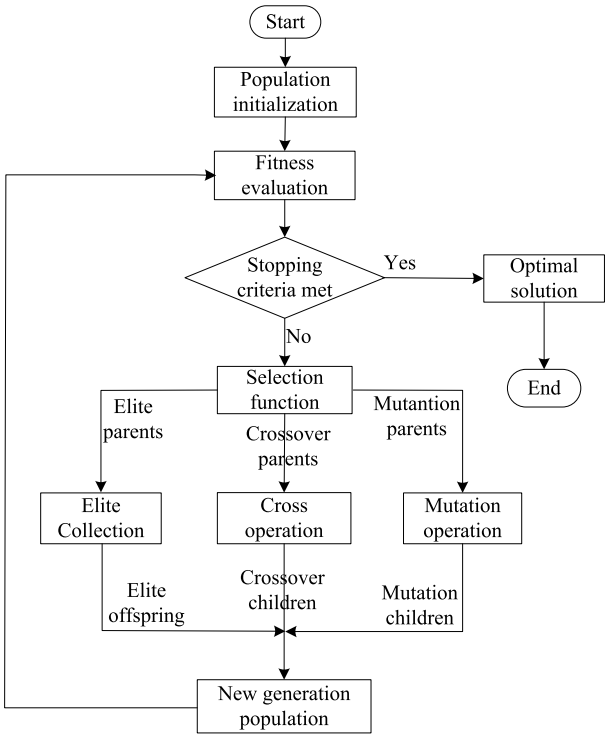

FIGURE 6. GA optimization flow chart.

energy storage system (P_{soc}), the formula (14) obtained is as follows:

$$P_{load}(k) + P_{soc}(k) = P_{wind}(k) + P_{grid}(k) \tag{14}$$

In the formula, $P_{wind}(k), P_{grid}(k), P_{fc}(k), P_{H_2O}(k), P_{load}(k)$ represents the wind power, grid power, fuel cell, electrolytic water consumption power and local load consumption power during k. Unit: kW.

In order to construct the state space representation, two state variables and one output variable are defined. As shown in formulas (15) and (16):

$$x_1(k) = ESOC_S(k) \tag{15}$$

$$x_2(k) = y(k) = P_{wind}(k) \tag{16}$$

Then the state space model can be expressed as:

$$x_1(k) = x_1(k-1) + \zeta_1 \cdot x_2(k) + \phi_1 \tag{17}$$

$$y_2(k) = x_2(k) \tag{18}$$

where ξ_1 is the conversion rate (i.e. the conversion rate between electricity and gas). ϕ_1 is a constant.

C. SOLUTION OF ROLLING OPTIMIZATION GA

In order to maximize the local consumption of local resources (wind energy) in the system, the purpose of system optimization is to minimize the transmission of electricity to the grid, so that most of the wind power is consumed locally.

TABLE 1. Simulation experiment parameters.

Parameter	Value
BP network structure	29-6-23-1
Vector η	0.1
Training target error	0.001
Training function	'trainlm'
Network structure activation function	'logsig', 'logsig', 'purelin'
Maximum Iterations K_{max}	100000
Acceleration factor $c_1 = c_2$	1.49445
Individual Location x_{min}, x_{max}	[-5 5]
Flight speed v_{min}, v_{max}	[-1 1]
Population size	100

Therefore, the objective function can be described as:

$$\begin{cases} f(k) = \min \sum_{k=0}^{24} P_{grid}(k) \\ s.t. \begin{cases} P_{load}(k) + P_{grid}(k) + P_{soc}(k) = P_{wind}(k) \\ 0.2 \le ESOC_S(k) \le 0.9 \\ 0.2 \le ESOC_H \le 0.9 \\ 0.2 \le ESOC_O \le 0.9 \\ 0 \le P_{wind}(k) \le P_{wind\,\max}(k) \\ 0 \le P_{soc}(k) \le P_{soc\,\max}(k) \\ 0 \le P_{grid}(k) \le P_{wind}(k) \end{cases} \end{cases} \tag{19}$$

where, $f(k)$ is the objective function at k time.$P_{wind\,\max}(k)$ is the maximum wind power at k time.$P_{soc\,\max}(k)$ is the maximum value of the equivalent state of charge of the energy storage system at k time.

In this paper, an optimization model has been established to maximize the local consumption of wind power to minimize the interaction between the system and the large power grid, including the objective function and various constraints. The specific optimization algorithm is genetic algorithm. The genetic algorithm calls the *ga* function, which aims at $ESOC_S$ to keep it in a safe range ($0.2 \sim 0.9$) while minimizing the fitness function. The goal of the fitness function is to minimize the interaction between it and the large power grid, that is, to make local power consumption as much as possible.

The fitness function will contain a variety of situations. After analyzing the power flow of the system, it is concluded that there are approximately 9 possible power flows, as shown in Fig. 5. Among these 9 types, there are appropriate or inappropriate ones. When the appropriate power flow comes, the punishment factor set for it is small, and for the inappropriate power flow, the punishment factor set for it is relatively large, for example, the most ideal situation is that the electricity generated by wind energy just meets the load demand, and

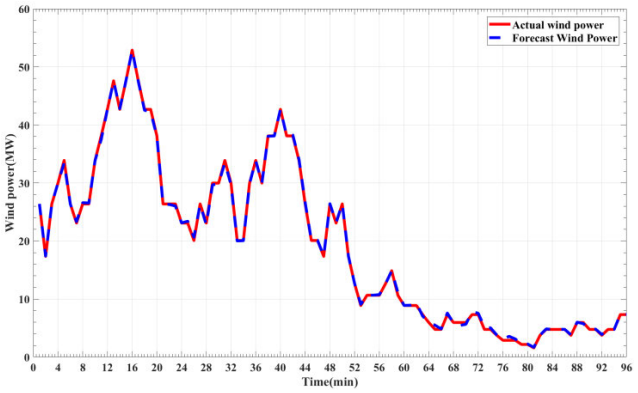

FIGURE 7. Comparison curve of wind power forecast output.

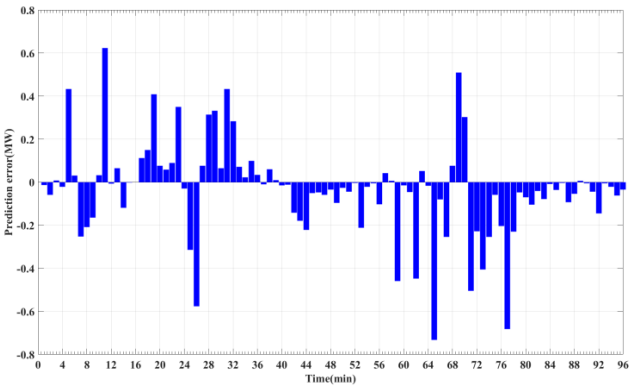

FIGURE 8. Wind power prediction error comparison curve.

the energy storage system $ESOC_S$ is between $0.2 \sim 0.9$, and the punishment factor is set to 0.

As described earlier, the genetic algorithm uses selection, crossover and mutation operators to search for the best candidate solution when its fitness function reaches the optimal value in the horizon. Its flow chart (Fig. 6). The steps of GA optimization are described as follows:

Step 1: The initial solution is generated. The initial solution is generated randomly between, for example, the state change in SSM can be expressed as $\{x(k)_{k=1\sim24} \mid [0.212, 0.301, 0.376, \ldots, 0.897]\}$;

Step 2: Calculation of fitness value. Each candidate solution is calculated by fitness function. The fitness function in this paper is composed of SSM function and a series of constraints. An SSM function represents the correlation between variables $x(k)$, $x(k-1)$ and $y(k)$defines constraints.

Step 3: Determination of termination conditions. If the candidate solution meets the end condition and the objective function at the same time, the optimal solution will be output out of the loop. Otherwise, two operators, crossover and mutation, are used to generate a new candidate solution, and then a new generation of genetic operator is generated through the action of GA, which returns to Step 2.

TABLE 2. Prediction performance analysis of prediction model.

	e_{MAPE}/%	RMSE	E
Improve PSO-BP	1.72	0.02	0.01

D. IMPLEMENTATION OF FEEDBACK CORRECTION

During the actual operation of the multi-energy flow system, because the reference value is based on the predicted value of the improved PSO-BP, there is a certain deviation between the optimal control scheme calculated by the rolling optimization and the optimal operation scheme of the actual system operation, as well as some external disturbances, the final predicted value cannot be consistent with the actual value, in order to make the predicted value and the actual value more similar, Therefore, the feedback adjustment link is added, and the actual value obtained each time is used as the basis, and the predicted value of the next time is used as the correction, so that the actual value of the next time is closer to the predicted value, to optimize and improve, so that the whole system becomes a closed-loop control optimization system, and the output value meets the requirements. The specific method is to measure the current actual state value of the system online, as the initial value of the rolling optimization at the current time, and continuously optimize the predicted output value according to the actual output value to form a closed-loop control to make the predicted output value more accurate.

$$\mathbf{x}(k+1) = \mathbf{x}_{real}(k+1) \tag{20}$$

where, $\mathbf{x}(k+1)$ is the initial value of wind power at k+1 time. $\mathbf{x}_{real}(k+1)$ is the wind power value at k time collected by the actual measurement system after the predicted wind power at k+1 time is issued.

V. EXAMPLE ANALYSIS

A. IMPROVED PSO-BP EXAMPLE ANALYSIS

The above model is applied, and in order to better verify the superiority and universal applicability of the model, the measured data of a wind farm in the Netherlands are used for research and analysis, and 96 data are observed every day with a sampling interval of 15 minutes. The wind power from March 1 to 29 is selected as the training sample (2784 data sets), and the wind power from March 30 is selected as the test sample (96 data sets). Other simulation experiment parameters are shown in Table 1.

Based on the parameters set above, the research sample is imported into the relevant design program, and the predicted wind power curve and actual wind power curve obtained are shown in Fig. 7. The corresponding prediction error curve is shown in Fig. 8.

It can be seen from the above figures that the prediction effect of the improved PSO-BP neural network combination model is good, but in order to more accurately

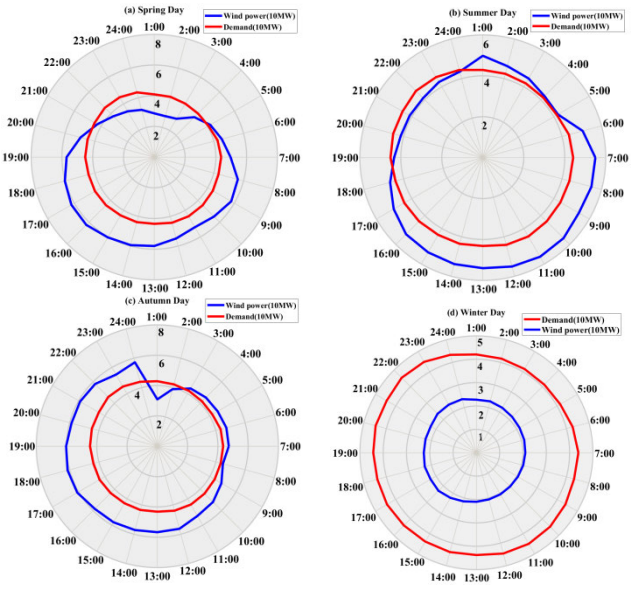

FIGURE 9. Daily power consumption and wind power diagrams.

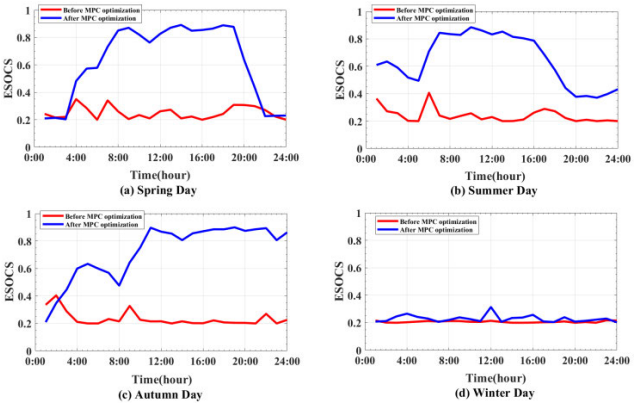

FIGURE 10. Comparison of ESOCS results.

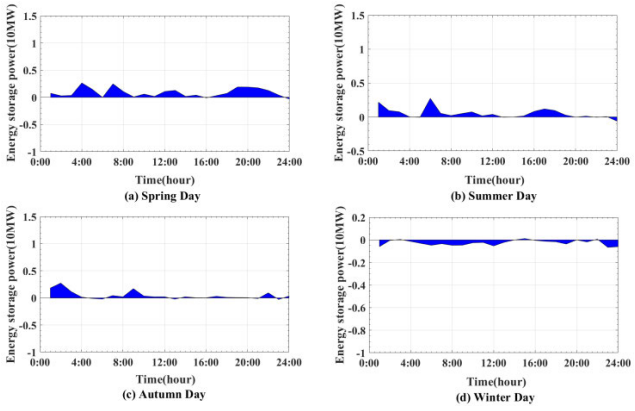

FIGURE 11. Comparison of power changes of energy storage system before MPC optimization.

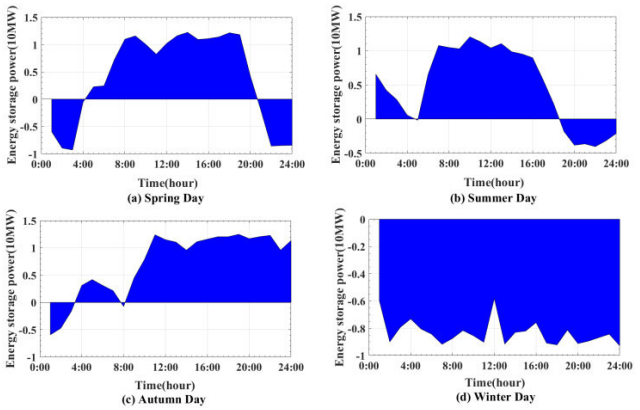

FIGURE 12. Comparison of power changes of energy storage system after MPC optimization.

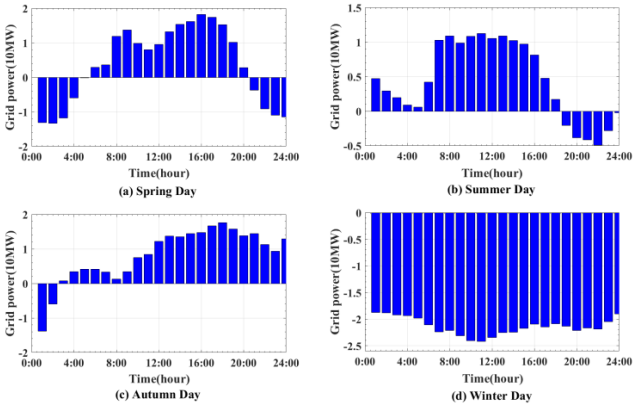

FIGURE 13. Comparison of interactive power changes before MPC optimization.

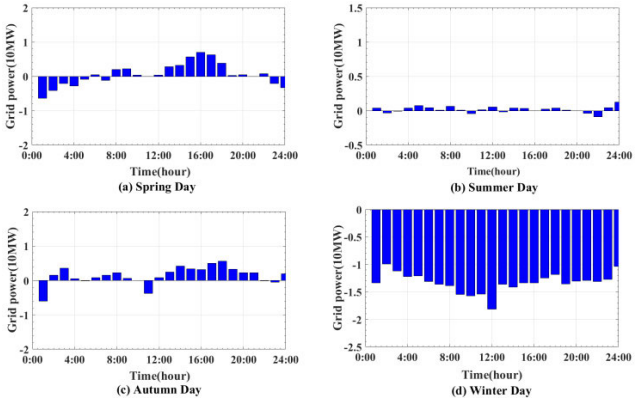

FIGURE 14. Comparison of interactive power changes after MPC optimization.

verify the accuracy of each prediction model, the article will use the average percentage error e_{MAPE}, root-mean-square error (RMSE) and relative entropy E (reflecting the ''close'' distance between the actual value and the predicted value), are used to improve the PSO-BP combination prediction model for performance evaluation (96 observation values are evaluated). The three evaluation indicators are defined as follows:

$$e_{MAPE} = \frac{1}{N}\sum_{k=1}^{N}\left|\frac{O(k) - T(k)}{O(k)}\right| \cdot 100\% \qquad (21)$$

$$RMSE = \sqrt{\frac{1}{N} \cdot \sum_{k=1}^{N} (O(k) - T(k))^2} \quad (22)$$

$$e_{MAPE} = \frac{1}{N} \sum_{k=1}^{N} \left| \frac{O(k) - T(k)}{O(k)} \right| \cdot 100\% \quad (23)$$

In the above formula, k is the time node, N is the number of predicted samples, $T(k)$ is the predicted value, and $O(k)$ is the actual value.

According to the prediction results of the above chart, the average percentage error, root-mean-square error and relative entropy are 1.72%, 0.02 and 0.01 respectively. The BP neural network optimized by improved PSO is closer to the historical data and the prediction is more accurate.

B. MPC STRATEGY EXAMPLE ANALYSIS

1) EXAMPLE DESCRIPTION

This paper takes the actual data of four different seasons and one day in a certain area of the Netherlands as an example to verify the feasibility and effectiveness of the proposed multi-energy flow system control method. The wind power and actual load predicted by improving PSO-BP, namely the actual daily power consumption and the predicted daily wind power (Fig. 9).

It can be seen from Fig. 8 that the load and wind power of the four seasons fluctuate within 24 hours, but as time goes on, the load shows some regularity. The power consumption is less between 1:00 and 6:00 every day, and more between 7:00 and 23:00. 7:00 and 20:00 are the most power consumption in a day, which can reach 54.92 MW and 58.69 MW respectively. However, wind power is extremely unstable, with the largest fluctuation in spring, ranging from 27.62MW to 62.48MW. Secondly, wind power fluctuates greatly in autumn, ranging from 30.88MW to 61.38MW. However, wind power fluctuates little in summer and winter, with the smallest fluctuation in winter, and the smallest wind power throughout the day (only 23.72MW at the maximum), which is less than the daily power consumption throughout the day.

Compared with the above figure, it is obvious that there is an obvious mismatch between supply and demand, because for this system, supply and demand are intermittent. Therefore, hydrogen energy storage system is needed to balance the difference between energy. This paper uses the MPC optimization strategy to maintain the optimal operation of the energy storage system while meeting the energy demand. In order to facilitate the study of the measured data, the data in Fig. 9 are processed and collected once in one hour.

2) RESULT ANALYSIS

In order to fully prove the feasibility and effectiveness of the MPC optimization method proposed in the article, that is, to achieve the goal of maximizing the local consumption of local wind power, under the same wind power and load, the paper intends to take the multi-directional flow control results of the non-optimized hydrogen energy storage system as a comparison. Therefore, the results of the calculation example are shown in Figs. 10 to 14.

Fig. 11 shows the comparison of the results of the four-day ESOCS test selected in the article. From the figure, it can be seen that the ESOCS is sometimes high and sometimes low within 24 hours, which is intended to temporarily store wind power when the system is rich in wind power, and discharge the required load when the wind power is scarce, to balance this demand relationship of the system, and then achieve local wind power consumption as far as possible. As shown in Fig. 10(a), the ESOCS after MPC optimization between 3:00 and 22:00 is greater than its value before optimization, and because the wind power is large and larger than the load demand during this period, so too much wind power is temporarily stored by the energy storage system, that is, more wind power is used to charge the energy storage system (electrolytic water for hydrogen production). Before MPC optimization, the ESOCS changes from 0.2 to 0.35, while after optimization, the ESOCS changes from 0.21 to 0.89. In Fig. 10(b), if the wind power decreases between 1:00 and 5:00, the energy storage system is in the discharge state in order to maintain the balance between supply and demand of the microgrid system, that is, the ESOCS decreases, and then the wind power increases and maintains a large level between 5:00 and 16:00, then the energy storage system starts to charge, that is, the ESOCS increases from 0.3 to 0.9, and then the wind power decreases, and the ESOCS decreases due to the discharge. Therefore, from the comparison in the figure, it can be seen that the optimized ESOCS can store more wind power temporarily, When the wind power is reduced, the load will be consumed, which increases the local consumption of wind power. For autumn, because the wind power is not big at first, the ESOCS fluctuates little. Until the wind power is big after 8:00, the ESOCS after MPC optimization remains around 0.9, while the ESOCS before MPC optimization fluctuates little, around 0.25. It can be seen from Figure 10d that because the wind power in winter is small all day and less than the load, the value of ESOCS is relatively small. Without optimization, although it fluctuates, its value almost remains at 0.2. Even under MPC optimization, the value of ESOCS also changes slightly, with a maximum of 0.3. In general, the change amplitude of ESOCS under MPC optimization is large.

Fig. 12 shows the result of energy storage system power without MPC optimization. It can be seen from the figure that before MPC optimization, the power in the energy storage system has little change, even when the wind power of the system is less than the load, it also has little effect. For example, at 5:00∼21:00 in spring and 5:00∼18:00 in summer, the maximum increase is 2.5MW, so the system can only request a large amount of supplementary power from the large grid. The power change of the energy storage system after MPC optimization is shown in Fig. 13. The energy storage system after MPC optimization has a strong

TABLE 3. Comparison and analysis of wind power consumption results in four seasons.

Seasonal type	Optimization method	Demand /MW	Wind power /MW	Grid power /MW	Wind power integrated into the grid /MW	Local absorption of wind power /%	Increase and absorb wind power /MW	Lifting rate /%
Spring	B	1041.69	1150.78	247.34	167.85	85.41	132.22	11.49
	A			58.57	35.63	96.90		
Summer	B	1052.46	1171.08	142.54	124.48	89.37	118.05	10.08
	A			8.82	6.43	99.45		
Autumn	B	1047.76	1254.84	236.60	216.80	82.72	171.78	13.69
	A			55.57	45.02	96.41		
Winter	B	1047.13	528.24	512.89	0	100	0	0
	A			318.50	0	100		
amount to	/	4189.04	4104.94	/	/	/	422.05	10.28

ability to temporarily store (charge positive, that is, electrolysis hydrogen production is positive. Discharge negative, fuel cell discharge is negative) wind power. Especially by comparing Figs. 11(d) and 12(d), it is clear that the maximum temporary storage wind power of the energy storage system before MPC optimization is 0.8MW, and most of the time is 0MW. After MPC optimization, the temporary storage wind power of the energy storage system is mostly above 8MW.

Figs. 13 and 14 show the comparison of the results of the interaction power between the system and the large power grid (combined as positive, from negative). From the overall view of the figure, the interaction power after MPC optimization is far less than the interaction power before MPC optimization, that is, to ensure the maximization of local wind power consumption. It can be seen from Figs. 13(a) and 14(a) that the change range of the unoptimized interactive power is −13.33∼18.21MW, with a span of 31.54MW, while the change range of the optimized interactive power is small, between −6.21∼7.02, with a span of only 13.23MW. In summer, because the wind power is more than the load most of the time, the energy storage system will be charged with the wind power that is not used up, and then the rest will be directly connected to the large grid. The interactive power variation amplitude between the system and the large grid will be 31.35 MW when the wind power is not optimized, and 11.63 MW after optimization, as shown in Figs. 13(b) and Figs. 14(b). Similar to summer in autumn, wind power is usually larger than the load, only between 1:00 and 3:00. When the system is not optimized, more power is integrated into the grid, with an average of about 10MW. After MPC optimization, due to the enhanced capacity of the energy storage system to cache wind power, less power is integrated into the large grid, with an average of about 2MW, as shown in Figs. 13(c) and 14(c). For winter, because the wind power is less than the load all day, the system has to apply to the power grid for power supplement all day, but the applied power supplement is significantly different before and after MPC optimization. The applied power supplement before MPC optimization is 512.89MW, and after MPC optimization, due to the increase of the temporary wind power storage capacity of the energy storage system, the applied power supplement is 318.50MW, and the applied power supplement before and after optimization is 194.39MW less, as shown in Figs. 13(d) and 14(d).

Therefore, in order to better see the degree of wind power consumption in spring, summer, autumn and winter, we will select the experimental data of the four seasons to analyze the specific wind power consumption, as shown in Table 3 below. Chart description: in the table, B represents before MPC optimization, and A represents after MPC optimization. "+" for energy storage refers to charging (hydrogen production by electrolysis of water), and "-" for energy storage refers to discharge (fuel cell discharge). The interactive power "+" refers to the connection to the large power grid, and "-" refers to the application for power supplement from the large power grid.

It can be seen from the above table that the total load in four seasons is 4189.04MW and the total wind power is 4104.94MW. After the optimization of the system, the wind power absorbed by the lifting system is 422.05MW, and the increase rate is 10.28%. Among them, the capacity of the system to absorb wind power after the optimization of the MPC method has been improved to varying degrees, with the local wind power consumption rate reaching 96.41%∼100%, and the increase of the wind power consumption rate in spring,

summer, autumn and winter is 11.49%, 10.08%, 13.69% and 0 respectively, except in winter, The capacity of absorbing wind power improved in the other three seasons is relatively obvious, and the reason for no improvement in winter is that wind power is far less than the load all day long (wind power is completely absorbed locally).

Based on the analysis of the above data, charts and results, it is known that the method of MPC optimization of multi-energy flow system can effectively maximize the local consumption of local resources (wind energy) while ensuring the stable operation of the system.

VI. CONCLUSION

To intake more wind power consumption in micro-grids, this paper establishes a practical analysis model and proposes a model predictive control method for a wind-hydrogen hybrid power generation system while studying and analyzing the output characteristics of each micro-source. 24-hour wind power is predicted through the improved PSO-BP neural network to achieve optimal scheduling. Genetic algorithm is used to solve the optimal solution within the optimal range over 24 hours, while SSM compares the predicted results with the measured data to adjust the control strategy.

The research results of this work are summarized as follows:

1) The proposed MPC optimization method increases the wind energy consumption by 10.28%.

2) by considering the intermittent characteristics from the both supply and demand sides, this paper makes full use of the energy storage system composed of electrolytic water device, hydrogen and oxygen storage tank and fuel cell to balance the supply and demand while maintaining the energy storage system within the safe range.

3) The effectiveness of this method is verified in a limited simulation environment. In the follow-up research work, the developed strategy will be implemented in an actual wind farm with fuel cell energy storage. A comprehensive test bed is also under development.

This technology provides a new method to operate grid-connected power generation with a purpose of effective use of intermittent renewable energy. This will promote the application of wind energy, hydrogen and fuel cells in power generation.

REFERENCES

[1] FCH JU. (Jun. 2019). *Hydrogen Roadmap Europe: A Sustainable Pathway for the European Energy Transition*. [Online]. Available: http:Power-to-Ships:Futureelectricityandhydrogendemandsforshippingonthe AtlanticcoastofEuropein2050

[2] China Daily Economy. *China Becomes the First Contributor for Hydrogen Production*. [Online]. Available: http://www.gov.cn/xinwen/2019-7/08/content_5407075.htm

[3] B. Liu, S. Liu, S. Guo, and S. Zhang, "Economic study of a large-scale renewable hydrogen application utilizing surplus renewable energy and natural gas pipeline transportation in China," *Int. J. Hydrogen Energy*, vol. 45, no. 3, pp. 1385–1398, Jan. 2020.

[4] D. Hammerstrom, J. Brous, D. Chassin, G. Horst, R Kajfasz, P. Michie, T. Oliver, T. Carlon, C. Eustis, O. Jarvegren, W. Marek, R. Munson, and R. Pratt, "Pacific Northwest GridWise testbed demonstration projects; Part II. Grid friendly appliance project," Pacific Northwest Nat. Lab., Richland, WA, USA, Tech. Rep., PNNL-17079, 2007.

[5] D. Apostolou and P. Enevoldsen, "The past, present and potential of hydrogen as a multifunctional storage application for wind power," *Renew. Sustain. Energy Rev.*, vol. 112, pp. 917–929, Sep. 2019.

[6] J. G. Romero, R. Ortega, and A. Donaire, "Energy shaping of mechanical systems via PID control and extension to constant speed tracking," *IEEE Trans. Autom. Control*, vol. 61, no. 11, pp. 3551–3556, Nov. 2016.

[7] P. K. Ray, S. R. Paital, A. Mohanty, Y. S. E. Foo, A. Krishnan, H. B. Gooi, and G. A. J. Amaratunga, "A hybrid firefly-swarm optimized fractional order interval type-2 fuzzy PID-PSS for transient stability improvement," *IEEE Trans. Ind. Appl.*, vol. 55, no. 6, pp. 6486–6498, Nov. 2019.

[8] E. Ahmadi Moghaddam, S. Ahlgren, C. Hulteberg, and Å. Nordberg, "Energy balance and global warming potential of biogas-based fuels from a life cycle perspective," *Fuel Process. Technol.*, vol. 132, pp. 74–82, Apr. 2015.

[9] P. D. Lund, J. Lindgren, J. Mikkola, and J. Salpakari, "Review of energy system flexibility measures to enable high levels of variable renewable electricity," *Renew. Sustain. Energy Rev.*, vol. 45, pp. 785–807, May 2015.

[10] J. Kluska and T. Zabinski, "PID-like adaptive fuzzy controller design based on absolute stability criterion," *IEEE Trans. Fuzzy Syst.*, vol. 28, no. 3, pp. 523–533, Mar. 2020.

[11] Y. Tiejiang, L. Guojun, and Z. Zengqiang, "Optimal modeling on equipment investment planning of wind power-hydrogen energy storage and coal chemical pluripotent coupling system," *Trans. China Electrotech. Soc.*, vol. 31, pp. 21–30, May 2016.

[12] S. Kohsri, A. Meechai, C. Prapainainar, P. Narataruksa, P. Hunpinyo, and G. Sin, "Design and preliminary operation of a hybrid syngas/solar PV/battery power system for off-grid applications: A case study in Thailand," *Chem. Eng. Res. Des.*, vol. 131, pp. 346–361, Mar. 2018.

[13] X.-C. Fan, W.-Q. Wang, R.-J. Shi, and Z.-J. Cheng, "Hybrid pluripotent coupling system with wind and photovoltaic-hydrogen energy storage and the coal chemical industry in Hami, Xinjiang," *Renew. Sustain. Energy Rev.*, vol. 72, pp. 950–960, May 2017.

[14] C. Luan, J. Cao, and C. Cheng, "Load control of heating unit based on model predictive control algorithm," *Thermal Power Gener.*, vol. 51, pp. 114–121, Jan. 2022.

[15] D. Molina, C. Lu, V. Sherman, and R. G. Harley, "Model predictive and genetic algorithm-based optimization of residential temperature control in the presence of time-varying electricity prices," *IEEE Trans. Ind. Appl.*, vol. 49, no. 3, pp. 1137–1145, May 2013.

[16] F. Xu, Q. Guo, and H. Sun, "Automatic voltage control of wind farms based on model predictive control theory," *Autom. Electr. Power Syst.*, vol. 39, pp. 59–67, Jan. 2015.

[17] L. Xie and M. D. Ilic, "Model predictive dispatch in electric energy systems with intermittent resources," in *Proc. IEEE Int. Conf. Syst., Man Cybern.*, Oct. 2008, pp. 42–47.

[18] B. Zhang, J. Chen, and W. Wu, "A hierarchical model predictive control method of active power for accommodating large-scale wind power integration," *Autom. Electr. Power Syst.*, vol. 38, pp. 6–14, Oct. 2014.

[19] D. Lei, C. Hui, and T. Pu, "Multi-time scale dynamic optimal dispatch in active distribution network based on model predictive control," *Proc. CSEE*, vol. 36, pp. 4409–4616, Jan. 2016.

[20] Z. Yan, Z. Tao, and L. Yajie, "Research on optimal energy management of home energy LAN based on model predictive control," *Chin. J. Electr. Eng.*, vol. 35, pp. 3656–3666, May 2015.

[21] X. Wei, Li Guanjun, and F. Chen, "Multi-time-scale energy management strategy for microgrid energy storage system containing sodium sulfide battery," *Power Grid Clean Energy*, vol. 32, pp. 160–166, Nov. 2016.

[22] Q. Fei, Y. Deng, H. Li, J. Liu, and M. Shao, "Speed ripple minimization of permanent magnet synchronous motor based on model predictive and iterative learning controls," *IEEE Access*, vol. 7, pp. 31791–31800, 2019.

[23] E. A. Al-Ammar, H. U. R. Habib, K. M. Kotb, S. Wang, W. Ko, M. F. Elmorshedy, and A. Waqar, "Residential community load management based on optimal design of standalone HRES with model predictive control," *IEEE Access*, vol. 8, pp. 12542–12572, 2020.

[24] Z. Zhang, "Research on economic optimal dispatching strategy of microgrid based on model predictive control," in *Proc. MATEC Web Conf.*, vol. 232, 2018, p. 01058.
[25] E. Mayhorn, K. Kalsi, M. Elizondo, W. Zhang, S. Lu, N. Samaan, and K. Butler-Purry, "Optimal control of distributed energy resources using model predictive control," in *Proc. IEEE Power Energy Soc. Gen. Meeting*, Jul. 2012, pp. 1–8.
[26] L. Yang, Q. Sun, N. Zhang, and Y. Li, "Indirect multi-energy transactions of energy internet with deep reinforcement learning approach," *IEEE Trans. Power Syst.*, vol. 37, no. 5, pp. 4067–4077, Sep. 2022.
[27] G. Zhang, F. Zhang, K. Meng, X. Zhang, and Z. Y. Dong, "A fixed-point based distributed method for energy flow calculation in multi-energy systems," *IEEE Trans. Sustain. Energy*, vol. 11, no. 4, pp. 2567–2580, Oct. 2020.
[28] Y. Li, D. W. Gao, W. Gao, H. Zhang, and J. Zhou, "Double-mode energy management for multi-energy system via distributed dynamic event-triggered Newton–Raphson algorithm," *IEEE Trans. Smart Grid*, vol. 11, no. 6, pp. 5339–5356, Nov. 2020.
[29] K. Yu, Z. Cen, X. Chen, C. Liang, Z. Zhou, Z. Dong, and L. Wu, "Optimization of urban multi-energy flow systems considering seasonal peak shaving of natural gas," *CSEE J. Power Energy Syst.*, vol. 8, no. 4, pp. 1183–1193, Jul. 2022.
[30] D. Qingxi, Y. Tiejiang, and M. Shengwei, "Energy coordination control strategy of wind power—Hydrogen energy storage and coal chemical multi-energy coupling system," *High Voltage Technol.*, vol. 44, pp. 176–186, Aug. 2018.
[31] T. Yuan, Q. Duan, X. Chen, X. Yuan, W. Cao, J. Hu, and Q. Zhu, "Coordinated control of a wind-methanol-fuel cell system with hydrogen storage," *Energies*, vol. 10, no. 12, p. 2053, Dec. 2017.
[32] L. Xing, X. Liu, T. Alaje, R. Kumar, M. Mamlouk, and K. Scott, "A two-phase flow and non-isothermal agglomerate model for a proton exchange membrane (PEM) fuel cell," *Energy*, vol. 73, pp. 618–634, Aug. 2014.
[33] L. Xing, P. K. Das, X. Song, M. Mamlouk, and K. Scott, "Numerical analysis of the optimum membrane/ionomer water content of PEMFCs: The interaction of Nafion® ionomer content and cathode relative humidity," *Appl. Energy*, vol. 138, pp. 242–257, Jan. 2015.
[34] L. Xing, Q. Cai, X. Liu, C. Liu, K. Scott, and Y. Yan, "Anode partial flooding modelling of proton exchange membrane fuel cells: Optimisation of electrode properties and channel geometries," *Chem. Eng. Sci.*, vol. 146, pp. 88–103, Jun. 2016.
[35] L. Xing, "An agglomerate model for PEM fuel cells operated with non-precious carbon-based ORR catalysts," *Chem. Eng. Sci.*, vol. 179, pp. 198–213, Apr. 2018.
[36] L. Xing, W. Shi, H. Su, Q. Xu, P. K. Das, B. Mao, and K. Scott, "Membrane electrode assemblies for PEM fuel cells: A review of functional graded design and optimization," *Energy*, vol. 177, pp. 445–464, Jun. 2019.
[37] X. Chen, W. Cao, Q. Zhang, S. Hu, and J. Zhang, "Artificial intelligence-aided model predictive control for a grid-tied wind-hydrogen-fuel cell system," *IEEE Access*, vol. 8, pp. 92418–92430, 2020.
[38] X. Yin, F. Cao, J. Wang, M. Li, and X. Wang, "Investigations on optimal discharge pressure in CO_2 heat pumps using the GMDH and PSO-BP type neural network—Part A: Theoretical modeling," *Int. J. Refrigeration*, vol. 106, pp. 549–557, Oct. 2019.
[39] Y. Zhang, N. Cui, Y. Feng, D. Gong, and X. Hu, "Comparison of BP, PSO-BP and statistical models for predicting daily global solar radiation in arid Northwest China," *Comput. Electron. Agricult.*, vol. 164, Sep. 2019, Art. no. 104905.
[40] Z. Qilong and C. Xiangping, "A genetic optimization method for considering wind power dissipation multivector flow systems," *Electr. Meas. Instrum.*, vol. 60, pp. 115–121, Mar. 2023.
[41] R. Jianlong, Z. Qiao'e, and Y. Zhiwei, "Prediction of wind power based on IPSO optimized fuzzy PSR-KELM model under big data," *Autom. Instrum.*, vol. 34, pp. 77–81, Nov. 2019.